

Supporting Information

How does Darunavir prevent HIV-1 protease dimerization?

Danzhi Huang* and Amedeo Caflisch*

^a Department of Biochemistry
University of Zürich, Winterthurerstrasse 190
CH-8057 Zürich, Switzerland
Phone: (+41 44) 635 55 21, FAX: (+41 44) 635 68 62
email: dhuang@bioc.uzh.ch
email: caflisch@bioc.uzh.ch

* Corresponding authors

keywords: molecular dynamics; binding free energy surface;
HIV protease; Darunavir; HIV resistance

April 5, 2012

PDB codes of 27 HIV-1 PR (mutants) complexed with DRV

1T3R, 1T7I, 2F80, 2F81, 2F8G, 2IDW, 2IEN, 2IEO, 3BVB, 3CYW, 3D1Z, 3D20, 3EKT, 3EM6, 3GGT, 3GGU, 3JVY, 3JW2, 3LZS, 3LZU, 3LZV, 3MWS, 3OXW, 3OY4, 3PWM, 3QOZ, 3SO9

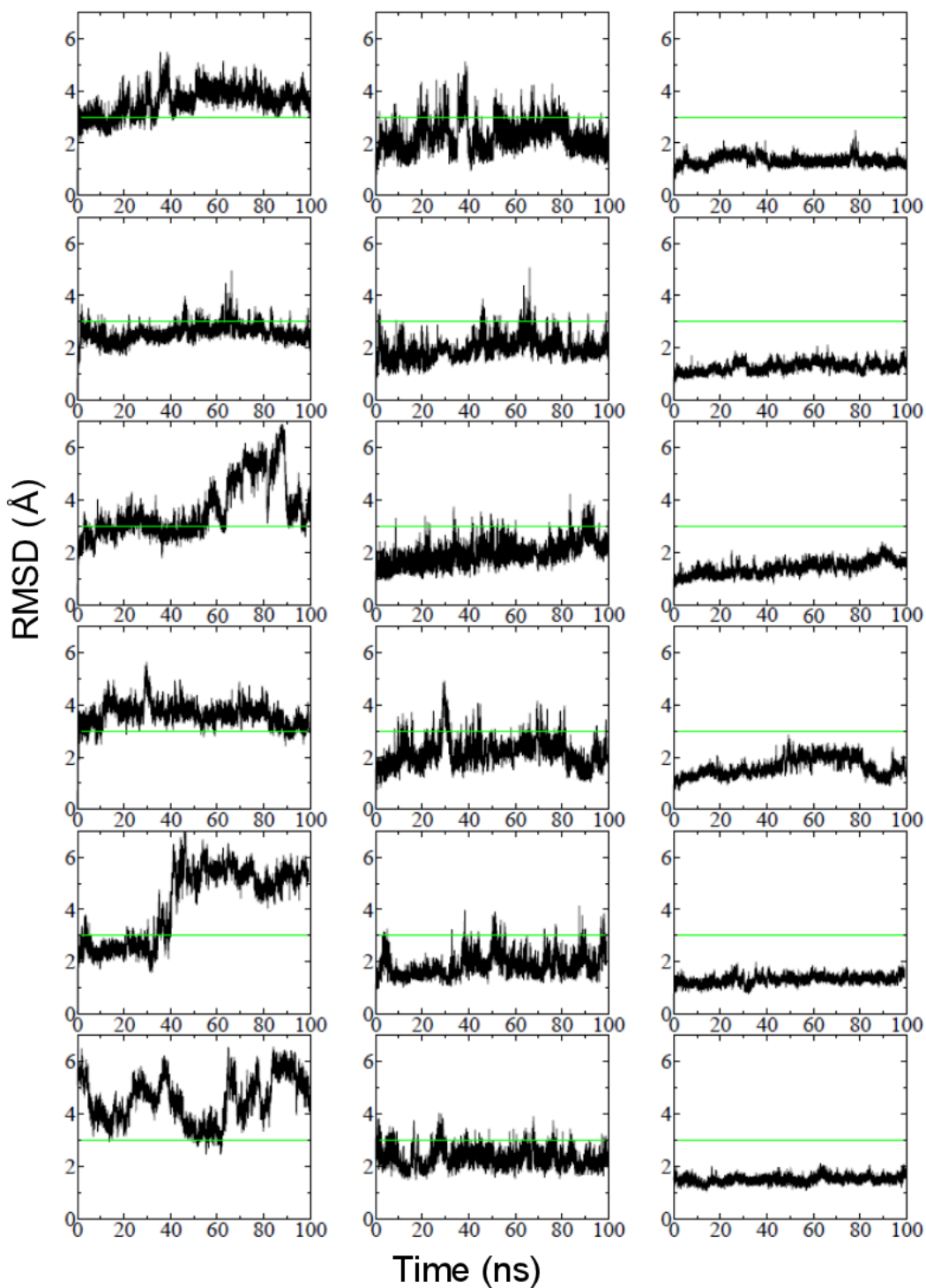


Figure 1: **Time series of RMSD of monomeric HIV-1 PR.** Three independent runs of V32I/L33I are shown in the three rows in the top half of the figure and three independent runs of V32I/L33F/I54M/V82I in the three rows in the bottom half. Left, middle, and right column correspond to all $C\alpha$ atoms, $C\alpha$ atoms of residues 11-90 (i.e., neglecting the termini), and $C\alpha$ atoms of residues 11-45 and 56-90 (i.e., neglecting termini and flap), respectively. These time series show that most of the monomeric structure is stable, and the most flexible parts are the N- and C-terminal segments (residues 1-10 and 91-99) followed by the flap (residues 46-55).

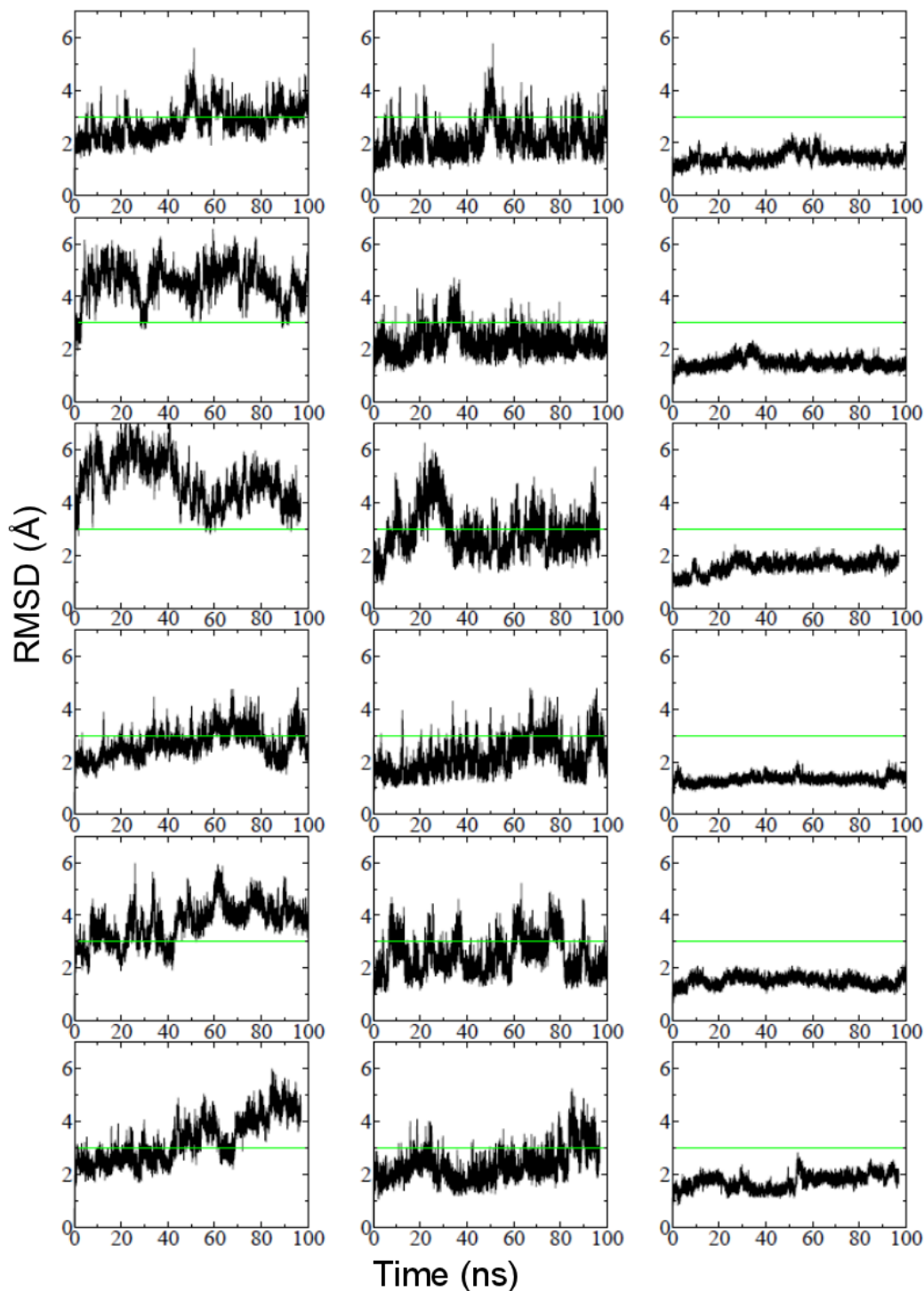


Figure 2: **Time series of RMSD of monomeric HIV-1 PR.** Three independent runs of V32I/L33F/I54M/V82A are shown in the three rows in the top half of the figure and three independent runs of V32I/L33F/I54M/I84V in the three rows in the bottom half. Left, middle, and right column correspond to all $C\alpha$ atoms, $C\alpha$ atoms of residues 11-90, and $C\alpha$ atoms of residues 11-45 and 56-90, respectively.

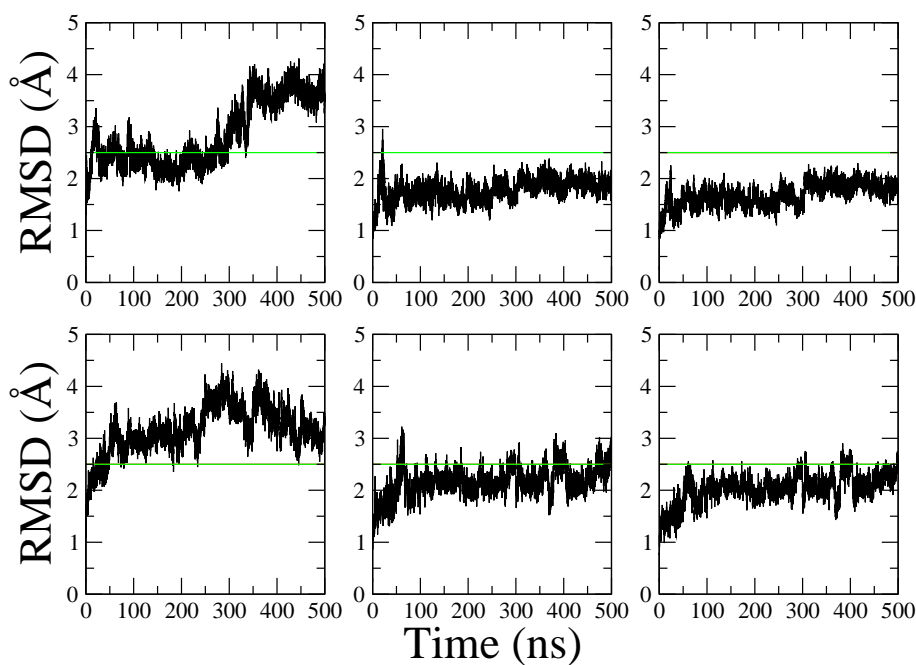


Figure 3: **Time series of RMSD of monomeric HIV-1 PR using the Amber force field.** Left, middle, and right column correspond to all $C\alpha$ atoms, $C\alpha$ atoms of residues 11-90, and $C\alpha$ atoms of residues 11-45 and 56-90, respectively. These two simulations with the Amber force field were started from the MD1 structure of V32I/L33I with bound DRV.

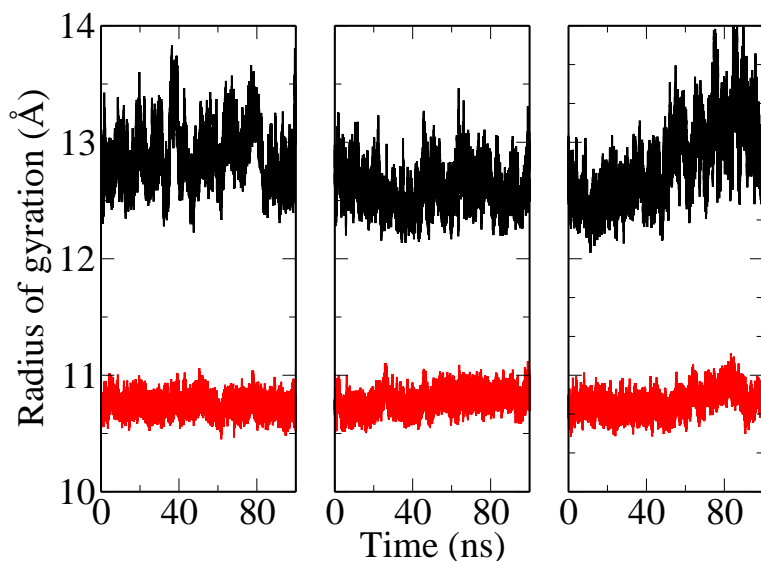


Figure 4: **Time series of radius of gyration.** Each panel shows one of the three independent runs of the V32I/L33I mutant of monomeric HIV-1 PR. The radius of gyration is calculated using the 99 $C\alpha$ atoms of monomeric HIV-1 PR (black) and neglecting the termini and flap, i.e., only for $C\alpha$ atoms of residues 11-45 and 56-90 (red). Note the larger fluctuations in the former.

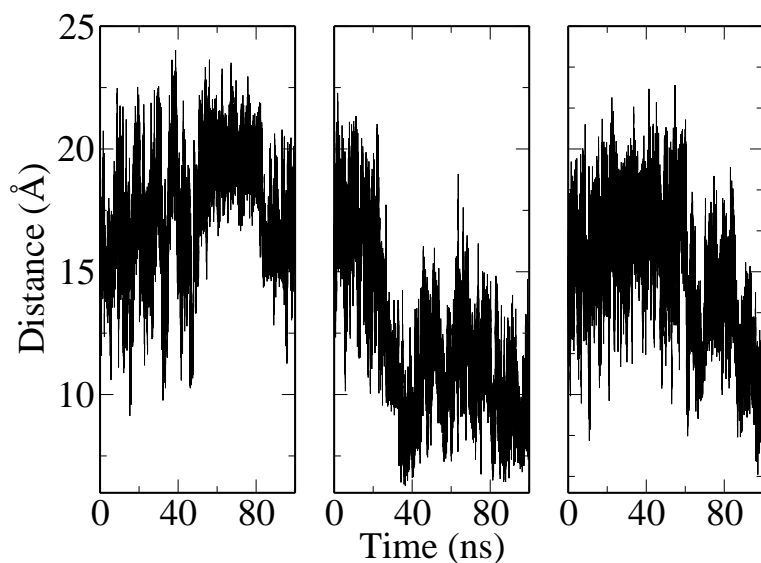


Figure 5: **Time series of distances from the $C\alpha$ atoms of residue Ile51 at the flap tip and residue Ile32 at the base of the active site.** Three independent runs of the V32I/L33I mutant of monomeric HIV-1 PR.

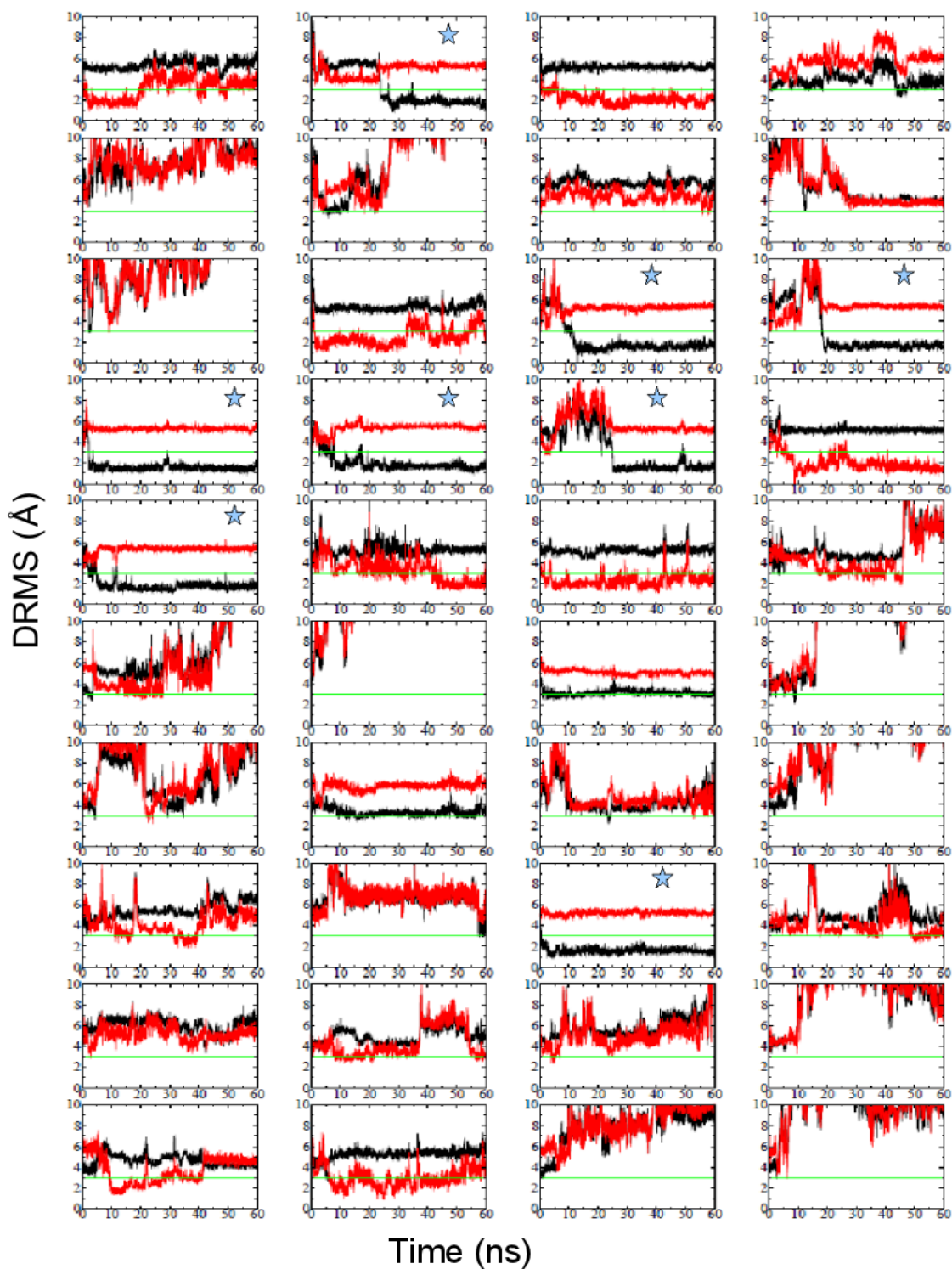


Figure 6: Time series of DRMS from the binding modes MD1 and MD2 of DRV into monomeric HIV-1 PR. Each panel shows the time series of DRMS from MD1 (black) and MD2 (red) for one of the 40 runs started from the X-ray structure of the complex (runs X1 and X2 in Table 1 of main text). The eight runs that reached the MD1 binding mode are emphasized by a cyan star.

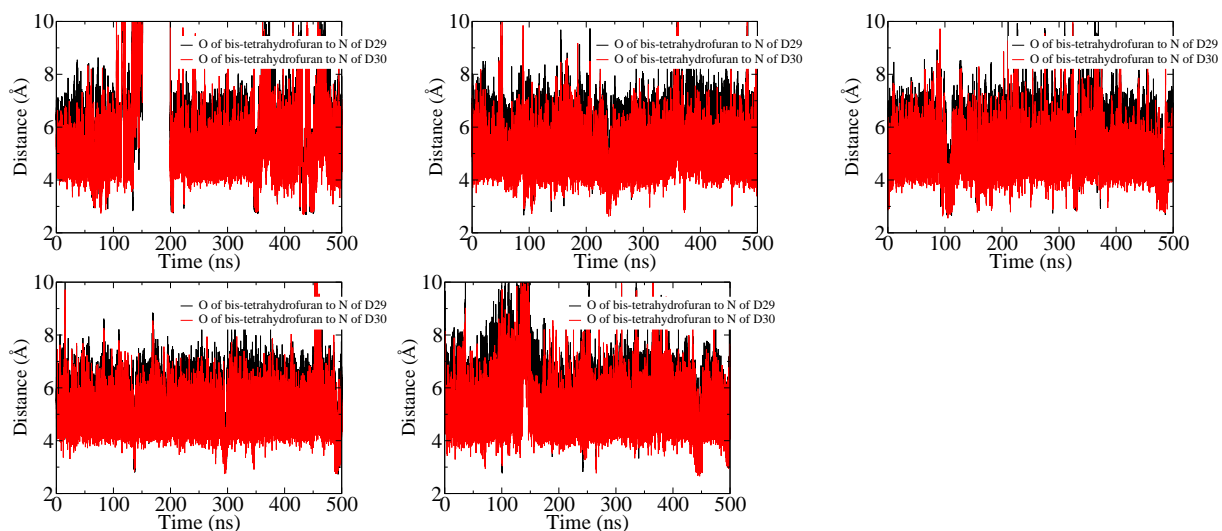


Figure 7: Distance of backbone amide nitrogen of residues 29 (black) and 30 (red) to the closest oxygen of the bis-tetrahydrofuran group of DRV in the $0.5\text{-}\mu\text{s}$ runs started from MD1.

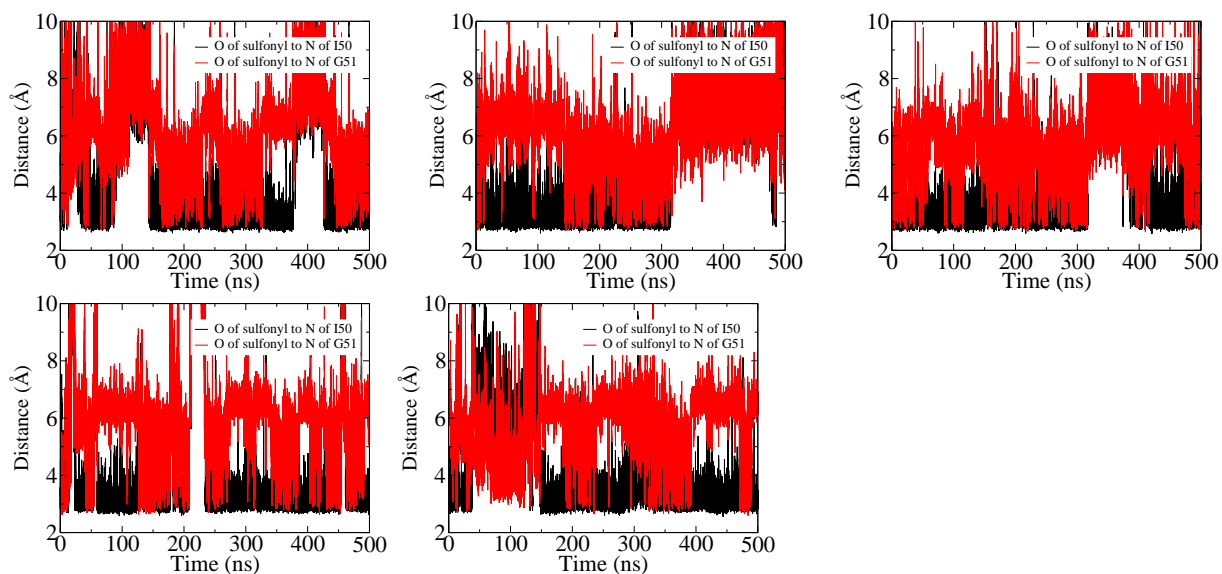


Figure 8: Distance of backbone amide nitrogen of flap residues 50 (black) and 51 (red) to the closest oxygen of the sulfonyl group of DRV in the $0.5\text{-}\mu\text{s}$ runs started from MD1.

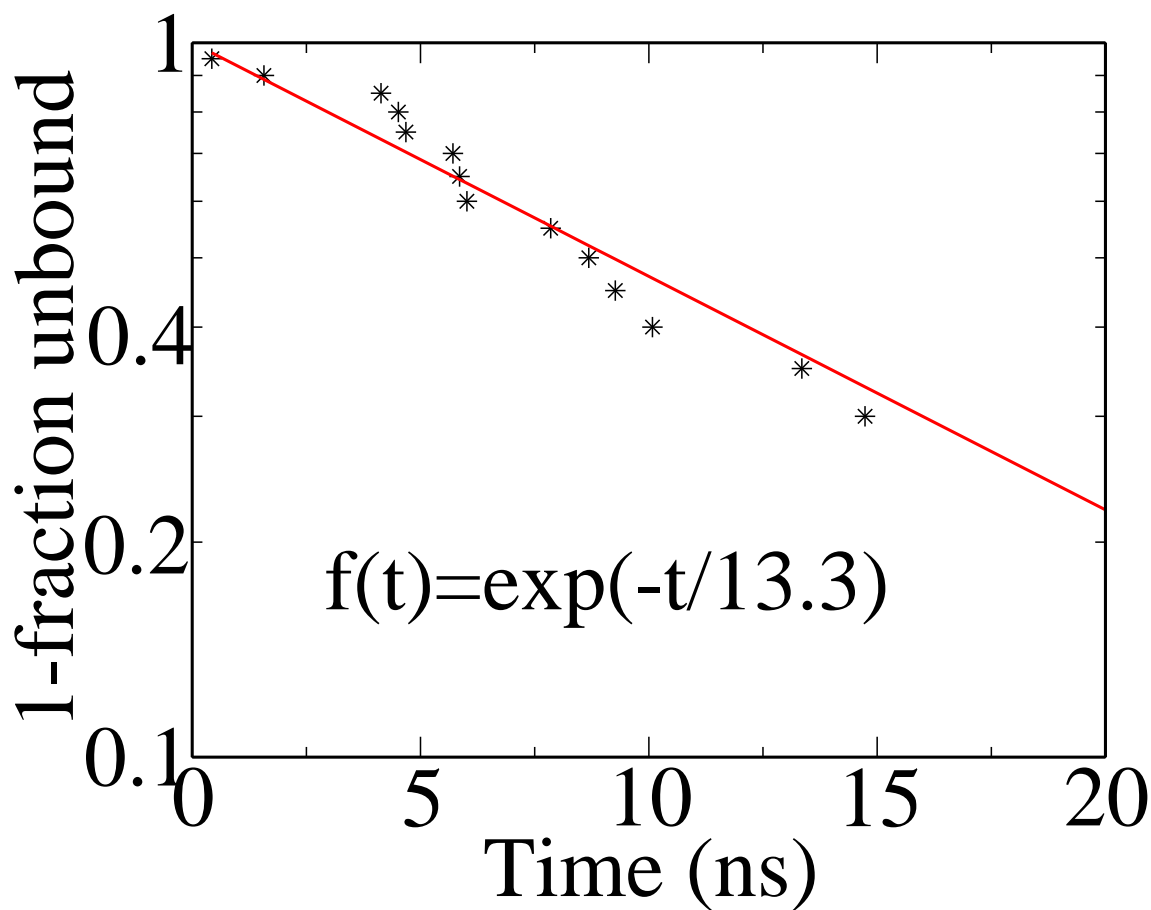


Figure 9: **Single-exponential kinetics of unbinding of DRV from the exterior surface of the flap of monomeric HIV-1 PR.** The plot shows the cumulative distribution $f(t)$ of the unbinding times for DRV from the flap binding site observed in the crystal structure of the complex with homodimeric HIV-1 PR (PDB code 2HS1). Note that only the monomer whose flap is in contact with DRV was used for these simulations which are called Xflap. There are 14 unbinding events within 20 ns in the 20 Xflap runs (see Table 1 in main text for a detailed description of the simulations).

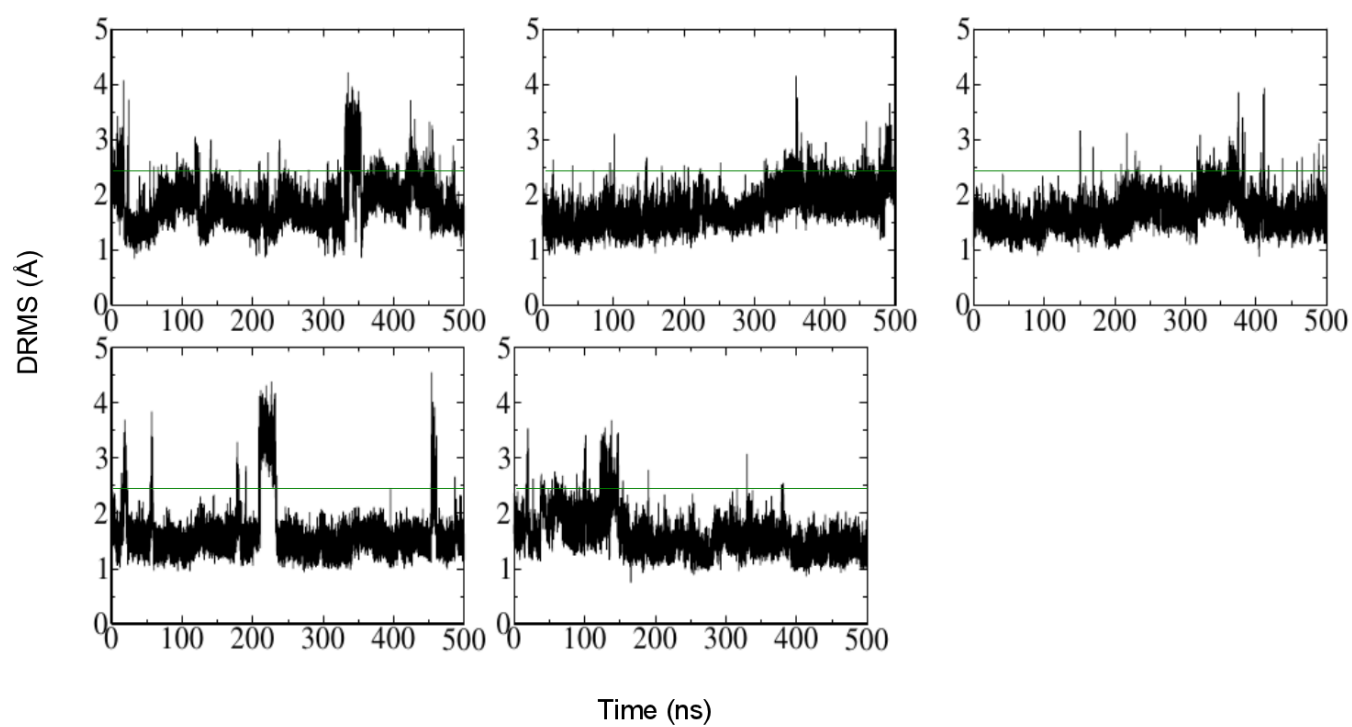


Figure 10: **Stability of the MD1 binding mode of DRV into monomeric HIV-1 PR.** DRMS are calculated using MD1 as reference.

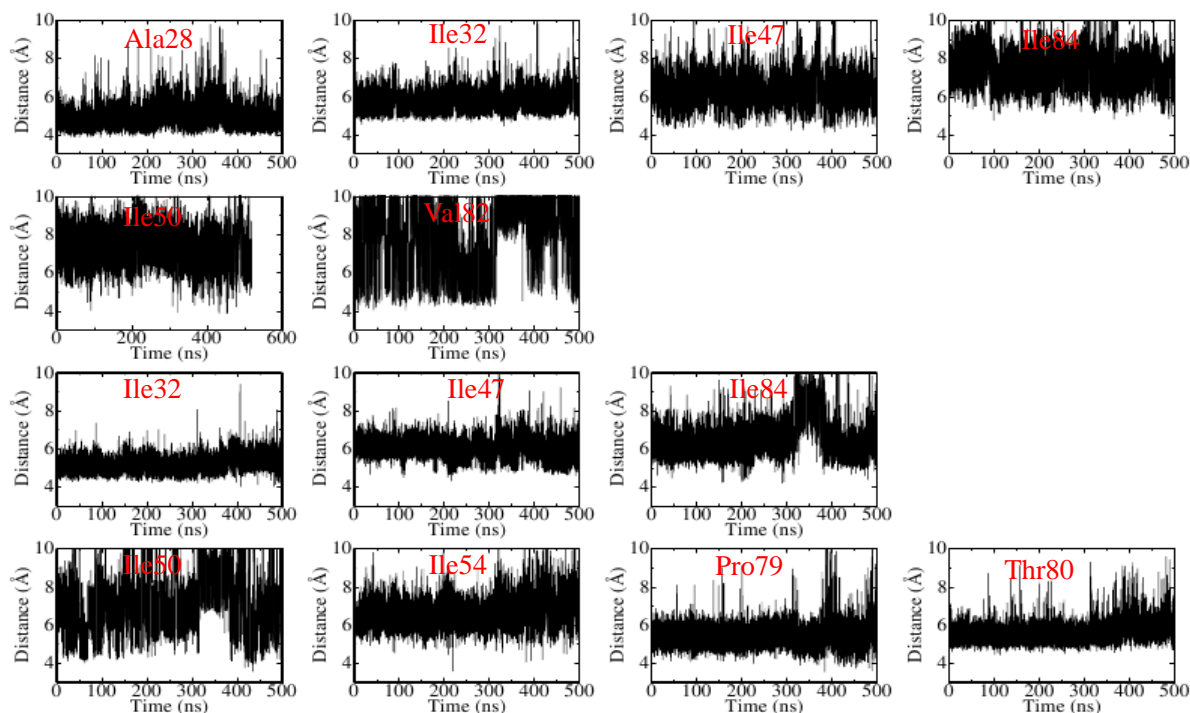


Figure 11: **Time series of hydrophobic contacts during one of the five 0.5- μ s simulations started from the MD1 binding mode.** Distances are between the centers of mass of the DRV functional groups and the side chains of monomeric HIV-1 PR. First row: bis-tetrahydrofuran to Ala28, Ile32, Ile47, and Ile84. Second row: phenyl group to Ile50 and Val82. Third row: isopropyl group to Ile32, Ile47 and Ile84. Fourth row: aniline group to Ile50, Ile54, Pro79, and Thr80. The other four 0.5- μ s simulations show qualitatively similar behavior.

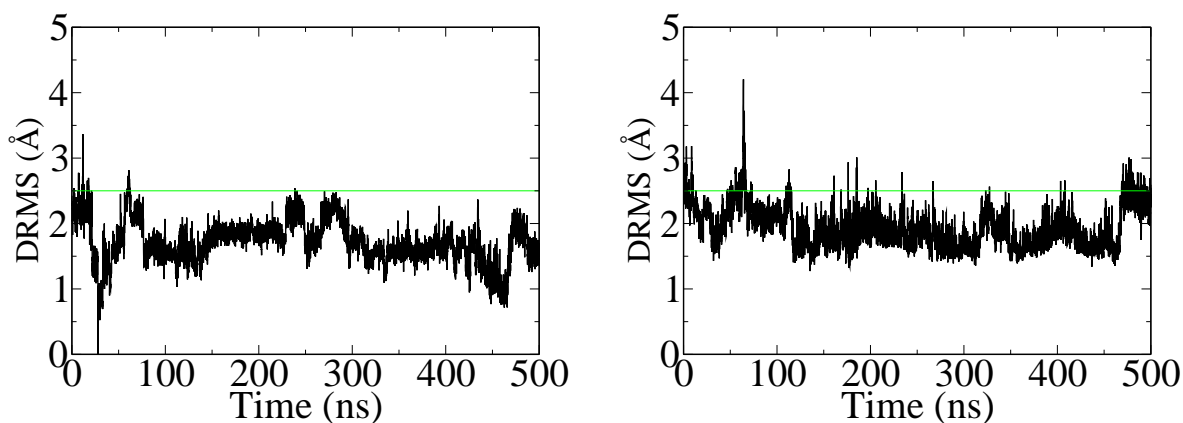


Figure 12: **Stability of the binding mode MD1 (obtained by the CHARMM PARAM22 force field) along the two 0.5- μ s simulations with the Amber force field.** DRMS are calculated using as reference the representative of the largest cluster sampled in the Amber simulations which is the snapshot at about 28 ns of the run in the left panel. The snapshots in the largest Amber cluster have a DRMS of about 2.2 Å from the MD1 binding mode.

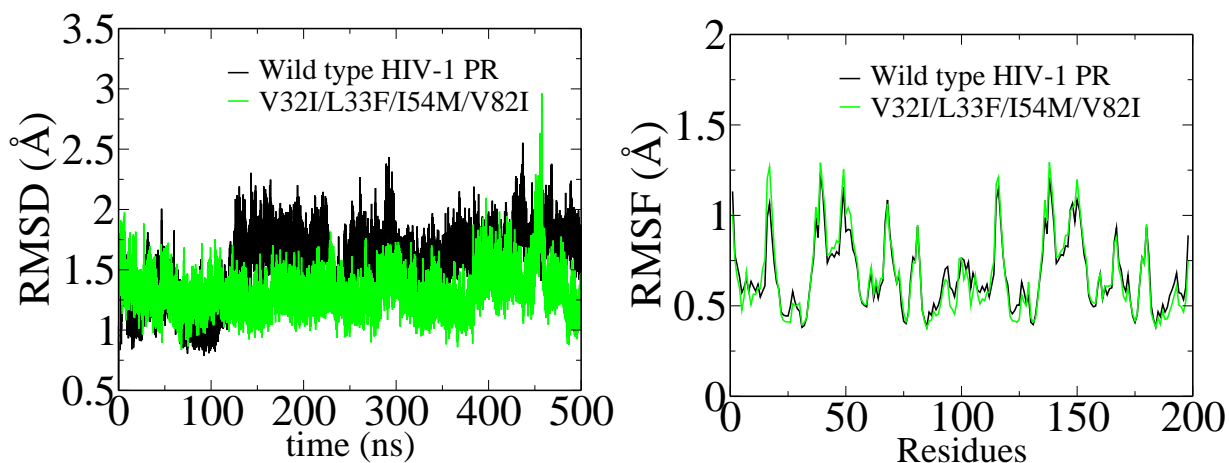


Figure 13: **Comparison of homodimeric wild type HIV-1 PR and the 8-point mutant V32I/L33F/I54M/V82I/V32'I/L33'F/I54'M/V82'I.** The same simulation set-up and protocols (with CHARMM22 force field) were used as for monomeric HIV-1 PR. The wild type simulation was started from the PDB structure 7UPJ (upon removal of the inhibitor). The simulation with the 8-point mutant was started from the PDB structure 2HS1 upon mutation of the side chains as explained in the main text. (Left) The RMSD was calculated using all of the 198 $C\alpha$ atoms of the homodimer and the initial PDB structure as reference. (Right) The RMSF values are average values over simulation intervals of 2 ns (excluding the first 20 ns). Note that the legends in both panels list only four of the eight mutations because of space.